Some properties of semiconducting $IrSb_3$

Glen A. Slack, and Veneta G. Tsoukala

Citation: Journal of Applied Physics **76**, 1665 (1994); doi: 10.1063/1.357750
View online: https://doi.org/10.1063/1.357750
View Table of Contents: http://aip.scitation.org/toc/jap/76/3
Published by the American Institute of Physics

Some properties of semiconducting $IrSb_3$

Glen A. Slack
GE Research and Development Center, Schenectady, New York 12301

Veneta G. Tsoukala
Oxford University, Oxford, England

(Received 26 October 1993; accepted for publication 9 April 1994)

Polycrystalline p-type samples of $IrSb_3$ and $Ir_{0.5}Rh_{0.5}Sb_3$ have been made by hot isostatic pressing of powders. A number of properties such as thermal expansion coefficient, sound velocity, thermal conductivity, electrical conductivity, Seebeck coefficient, and carrier concentration have been measured. These compounds show promise as thermoelectric materials.

I. INTRODUCTION

Iridium triantimonide, $IrSb_3$, is one of a number of compounds with the $CoAs_3$ or skutterudite structure.[1–3] Its semiconducting properties were first reported by Hulliger[4] in 1961. Recent band-structure calculations[5] confirm the semiconducting nature of these compounds. The covalent nature of the bonding was first pointed out by Pauling and Huggins[6] in 1934. A recent study by Caillat *et al.*[7] has been devoted to its thermoelectric properties. The $IrSb_3$ phase diagram has been studied by Kuzmin *et al.*.[8] The peritectic decomposition temperature is 1126 °C.[7] In the present study we have undertaken to measure several more properties of $IrSb_3$.

II. SAMPLE PREPARATION

We have prepared samples of $IrSb_3$ by reacting Ir (99.95% pure) and Sb (99.9999% pure) powder at 900 °C for 70 h. The powder was held in a chemically vapor deposited 2-cm-diam, 6-cm-tall BN crucible which itself was sealed inside an evacuated, fused quartz ampule. This ampule was heated in an external atmosphere of flowing argon in order to prevent the inward diffusion of air and water vapor during the run. After removal the resultant powder was sealed inside of an evacuated Pyrex ampule and placed in a hot isostatic press where it was consolidated at 940 °C for 1 h at 20 000 lb/in.^{2} of argon pressure. The resultant body was 98% dense and contained 1.5 μm-diam pores. It had a grain size of 6 ± 2 μm. Metallographic and electron-beam microprobe examination of the polished surface indicated that the sample contained 3 vol % of the $IrSb_2$ phase. Thus the stoichiometry of the $IrSb_3$ phase was at the Ir-rich phase boundary. A second sample with composition $Ir_{0.5}Rh_{0.5}Sb_3$ was made by reacting the starting powders at 850 °C for 340 h in a similar fused quartz ampule. The rhodium was 99.95% pure. It was hot isostatically pressed at 850 °C for 1 h at 25 000 lb/in.^{2}. The samples were both p type. The acceptors in both samples presumably come from the residual impurities in the iridium (or rhodium) which contained, in atomic parts per million, Si at 440, Fe at 150, Ru at 95, and Pb at 37. If each one of these impurity atoms produces one acceptor, the calculated carrier concentration in the $IrSb_3$ is 0.72×10^{19} cm^3. This is close to the carrier concentration calculated from the Hall effect.

III. EXPERIMENTAL DATA

A. X-ray measurements

We have measured the room-temperature x-ray lattice parameter of powdered $IrSb_3$ using powdered silicon as an internal standard. The result is $a_0=9.2503\pm0.0003$ Å. This result is in good agreement with the literature data of Zhuravlev and Zhdanov,[2] Kjekshus and Pedersen,[3] Kjekshus,[9] and Hulliger.[4] However, Kjekshus and Rakke[10] found a noticeably larger lattice parameter. It may be that some excess antimony can be trapped in the large vacant sites in the structure if the material is made with excess antimony thus enlarging the unit cell parameter. The present material was made at the Ir-rich phase boundary, and so should have the lowest possible lattice parameter.

The temperature dependence of a_0 was measured from 85 to 773 K with x-rays using copper K_α radiation. Silicon powder was again used as an internal standard, and this mixed with $IrSb_3$ powder was held on a tungsten strip heater in a helium atmosphere. The results are shown in Fig. 1 as crosses with the appropriate error bars. The data of Kjekshus[9] are shown as circles. From 300 to 673 K the thermal expansion is linear with

$$\alpha=6.6_5\times10^{-6}\ \text{K}.$$

The data of Kjekshus[9] suggest that there is a sudden decrease in α above 700 K which continues to 1250 K. Our data do not cover enough of this temperature range to enable us to comment on this effect.

B. Ultrasonic measurements

We have measured the ultrasonic wave velocity at room temperature in the polycrystalline compact of $IrSb_3$ which is 98% dense. A frequency of 5–10 MHz was employed. The sample thickness was about ten wavelengths. The results are

$$v(\text{longitudinal})=4.675(5)\times10^5\ \text{cm/s}.$$

$$v(\text{transverse})=2.717(5)\times10^5\ \text{cm/s}.$$

Using these values, the x-ray density, and the formulas of Anderson[11] we have calculated an adiabatic bulk modulus of

$$B_s=112.4\ \text{GPa}.$$

Poisson's ratio is calculated to be

$$\sigma=0.58.$$

 0021-8979/94/76(3)/1665/7/$6.00

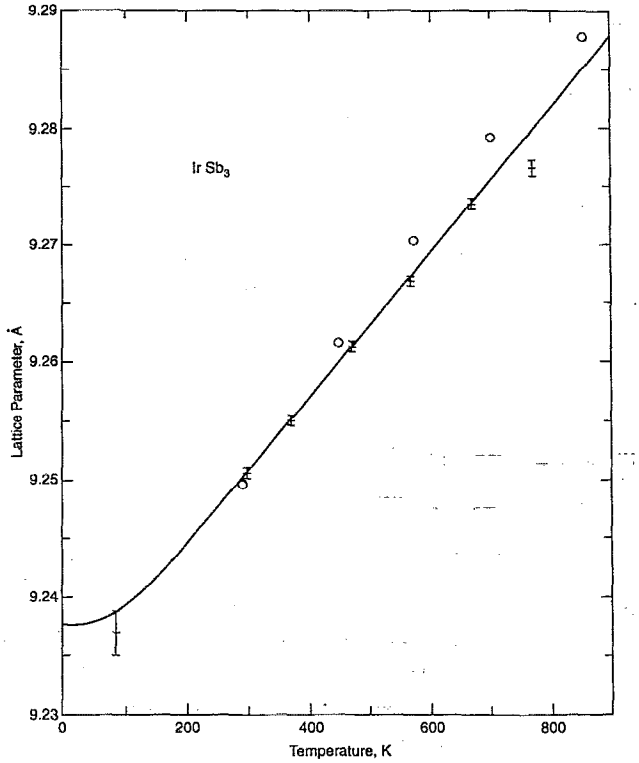

FIG. 1. The x-ray lattice parameter of $IrSb_3$ as a function of temperature. The crosses are the present data, the circles are from Ref. 9. The solid line was calculated from a simple Debye model.

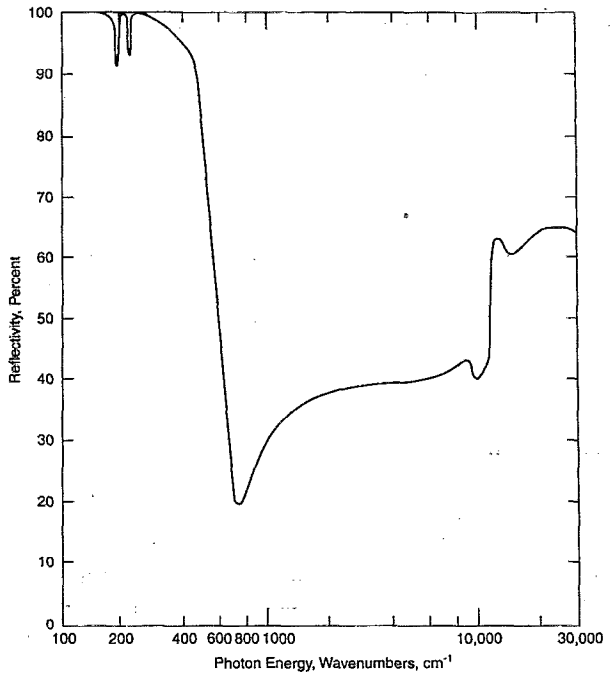

FIG. 2. The normal incidence reflectivity of $IrSb_3$ at room temperature as a function of the photon energy in wave numbers.

C. Optical measurements

The polycrystalline sample of $IrSb_3$ was mechanically polished to give a good specularly reflecting surface. Then the near-normal incidence reflectivity in the visible and infrared was measured at room temperature. We used a Nicolet model No. 740 Fourier transform infrared spectrometer. The results are shown in Figs. 2 and 3. Figure 3 is an expanded section of Fig. 2 for the region $100 \leqslant \tilde{\nu} \leqslant 220$ cm^{-1}. The reflectivity dips in Fig. 2 correspond[12,13] to transverse optical phonons at the zone center, while the data above $\tilde{\nu}=220$ cm^{-1} in Fig. 2 are associated with electronic effects. The onset of optical band-gap effects above 11 500 cm^{-1} are clearly seen. From this we estimate the band gap to be

$$E_g = 1.4 \text{ eV}.$$

In the case of $CoSb_3$ electrical conductivity measurements at high temperature[14] give $E_g=0.5$ eV.

We attempted to measure the optical transmission of thin sections of the $IrSb_3$ and $Ir_{0.5}Rh_{0.5}Sb_3$ specimens. Our conclusion was only that at $\tilde{\nu} \simeq 10\,000$ cm^{-1} the optical absorption coefficient was greater than 80 cm^{-1}, the samples were opaque.

D. Thermal conductivity measurements

We have measured the thermal conductivity K of the two polycrystalline samples, $IrSb_3$ and $Ir_{0.5}Rh_{0.5}Sb_3$, from 300 to 720 K. The results are shown in Fig. 4. The value of $K_g=0.160$ W/cm K at 300 K for $IrSb_3$ and varies as

$$K_g \sim T^{-1.3}.$$

For $Ir_{0.5}Rh_{0.5}Sb_3$ the value of $K_g=0.091$ W/cm K at 300 K and varies as

$$K_g \sim T^{-1.0}.$$

A small correction for the electronic contribution to the thermal conductivity has been made. The uncorrected K vs T curves are given in Fig. 5.

Figure 4 also gives literature data for the lattice thermal conductivity of single crystals of PbTe[15–18] and InSb.[19]

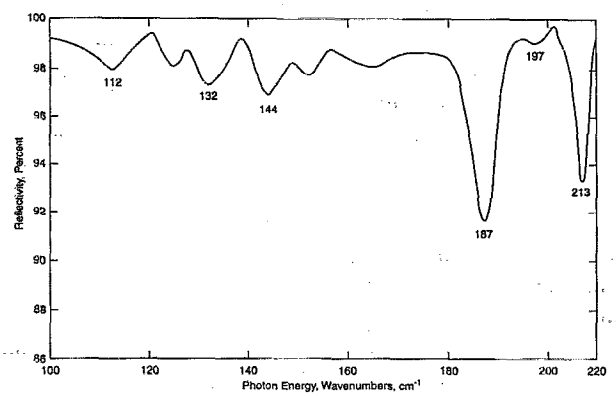

FIG. 3. The normal incidence reflectivity of $IrSb_3$ at room temperature in the far infrared as a function of the photon energy in wave numbers. The reflectivity dips correspond to transverse optical lattice modes.

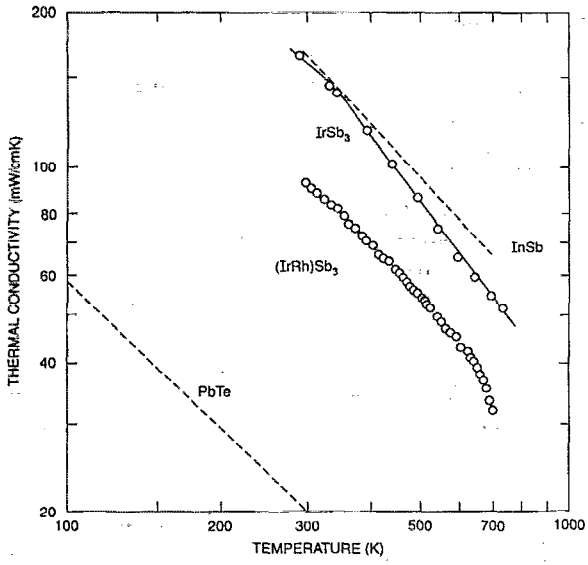

FIG. 4. The lattice thermal conductivity of polycrystalline $IrSb_3$ and $(Ir\text{-}Rh)Sb_3$ as a function of temperature. The dashed-line curves are literature data for single-crystal InSb and PbTe (see Refs. 15–19).

E. Electrical measurements

We are interested in the thermoelectric properties of $IrSb_3$ and have therefore measured the electrical resistivity and the absolute Seebeck coefficient of the two polycrystalline samples from 300 to 810 K. The resistivity data are given in Fig. 6, where $\rho=4.4\times10^{-4}$ Ω cm for $IrSb_3$ and 4.7×10^{-4} Ω cm for $Ir_{0.5}Rh_{0.5}Sb_3$ at 300 K. The Seebeck coefficient data are given in Fig. 7, where $S=+72\times10^{-6}$ V/K for $IrSb_3$ and $S=+58\times10^{-6}$ V/K for $Ir_{0.5}Rh_{0.5}Sb_3$ at 300 K.

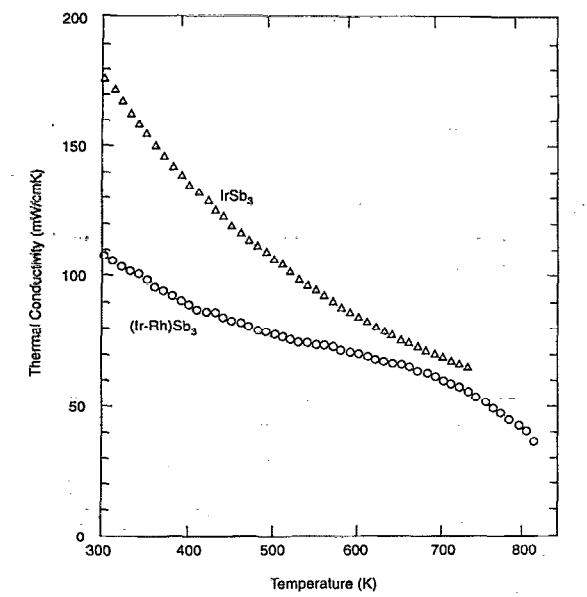

FIG. 5. The total lattice plus electronic thermal conductivity of $IrSb_3$ and $Ir_{0.5}Rh_{0.5}Sb_3$ as a function of temperature.

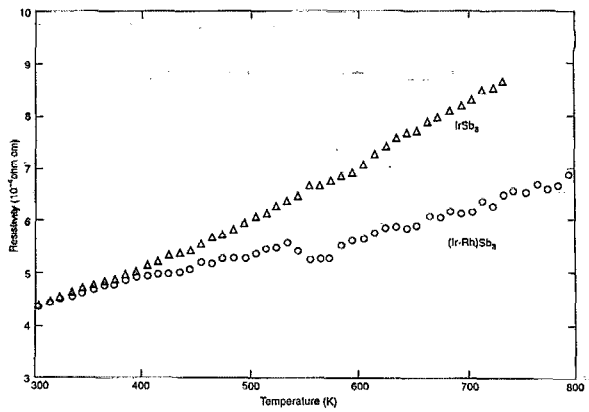

FIG. 6. The electrical resistivity vs temperature for $IrSb_3$ and $Ir_{0.5}Rh_{0.5}Sb_3$.

Measurements of the Hall coefficients showed both samples were p type. The data gave carrier concentrations and carrier mobilities at 300 K of $1.1\times10^{19}/cm^3$ and 1320 cm^2/V s for $IrSb_3$ and $0.67\times10^{19}/cm^3$ and 2120 cm^2/V s for $Ir_{0.5}Rh_{0.5}Sb_3$.

The experimental data on the two different samples are summarized in Table I.

IV. DATA ANALYSIS AND COMPUTATIONS

A. Figure of merit

The thermoelectric figure-of-merit Z has been calculated from

$$Z=S^2\sigma/(K_e+K_g).$$

The values as a function of temperature for the two samples are given in Fig. 8.

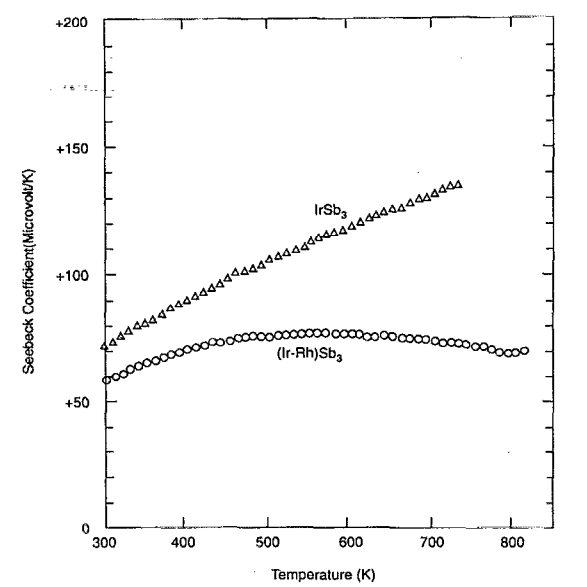

FIG. 7. The Seebeck coefficient vs temperature for $IrSb_3$ and $Ir_{0.5}Rh_{0.5}Sb_3$.

TABLE I. Experimental data at room temperature on polycrystalline $IrSb_3$ samples.

Quantity	Units	$IrSb_3$ p type	$Ir_{0.5}Rh_{0.5}Sb_3$ p type
σ	$\Omega^{-1}\,cm^{-1}$	2330	2280
μ (Hall)	$cm^2/V\,s$	1320	2120
μ (opt)	$cm^2/V\,s$	3050	···
p	$10^{19}/cm^3$	1.1	0.67
S	$\mu V/K$	72	56
(m^*/m_0)(opt)	···	0.12	
(m^*/m_0)(elec)		0.17	0.093
U(opt)	$cm^2/V\,s$	127	···
U(elec)	$cm^2/V\,s$	90	60
E_g	eV	1.4	···
K_g	mW/cm K	160	90
Grain size	μm	6±2	···
a_0	Å	9.2503(3)	9.2318(2)
X-ray density	g/cm^3	9.356	8.658
Bulk density	g/cm^3	9.16±0.03	···
Porosity	%	2	···
Pore size	μm	1.5	···
Long. velocity	10^5 cm/s	4.675	···
Trans. velocity	10^5 cm/s	2.717	···

B. Thermal expansion and Grüneisen parameter

The Grüneisen parameter γ of a solid can be calculated from the linear thermal expansion coefficient α by employing[20]

$$\gamma = 3\alpha B_T V_m / C_v , \tag{1}$$

where B_T=the isothermal bulk modulus, V_m=the molar volume, and C_v=the specific heat capacity per mole at constant volume. The isothermal bulk modulus B_T is related to the adiabatic bulk modulus B_s by

$$B_T = \frac{B_s}{1+\alpha\gamma T} . \tag{2}$$

At room temperature we have determined that B_s=112.4 GPa. Using the self-consistent value of γ derived from Eq. (1) we calculated that B_T=112.1 GPa. The value of C_v has been calculated from Beattie's tables[21] by assuming that $IrSb_3$ is a simple Debye solids with Debye temperature of θ=308 K. This value has been calculated from the sound velocity measurements. The resultant value of γ at room temperature from Eq. (1) is

$$\gamma = 1.42. \tag{3}$$

This value is intermediate between that of the perovskite, $SrTiO_3$, which has[22] $\alpha = 9.11\times10^{-6}$/K and γ=1.72, and InSb which has[23] γ=0.58. In InSb all the atoms are 4-coordinated, in $IrSb_3$ the Sb atoms are 4-coordinated while the Ir atoms are 6-coordinated. In $SrTiO_3$ the Sr is 12-coordinated, the Ti is 6-coordinated and the oxygen is 6-coordinated. The higher the average coordination number the larger the γ values tend to be. So the γ value of 1.42 appears to be reasonable for this mixed coordination number.

If we now assume that γ is independent of temperature, and that C_v is given by the simple Debye model, we can calculate the linear thermal expansion versus temperature. The solid curve shown in Fig. 1 was calculated in this way, and shows reasonable agreement with the measured x-ray lattice parameter versus temperature. The estimated lattice parameter of $IrSb_3$ at absolute zero is a_0=9.2377(5) Å.

C. Debye temperature

The Debye temperature can be calculated from the measured sound velocities by employing Anderson's expression[11]

$$\theta = 297.72(\bar{v}/\delta), \tag{4}$$

where θ is in K, $\bar{v}$ is in 10^5 cm/s, and δ^3 is the average volume per atom in 10^{-24} cm^3. The average sound velocity, $\bar{v}$ is determined from

$$\frac{3}{(\bar{v})^3} = \frac{2}{v_T^3} + \frac{1}{v_L^3} . \tag{5}$$

The result is

$$\theta = 308 \text{ K}.$$

D. Thermal conductivity

A theoretical estimate of the value of the lattice thermal conductivity at the Debye temperature, $K'(\theta)$, can be made using the analysis of Slack.[24] The prime denotes the theoretical value. The formula is

$$K'(\theta) = \frac{B\bar{M}\delta\theta^2}{n^{2/3}\gamma^2} , \tag{6}$$

where $\bar{M}$=the average mass of an atom of the crystal, δ^3=the average volume occupied by an atom, θ=the Debye temperature, n=number of atoms in the primitive unit cell, γ=the Grüneisen parameter at $T=\theta$, and $B = 3.04\times10^7$ $s^{-3}\,K^{-3}$. For the skutterudite structure[25] n=16. The theoretical result is

$$K'(\theta) = 94 \text{ mW/cm K}.$$

The measured lattice thermal conductivity at 308 K is

$$K = 156 \text{ mW/cm K}$$

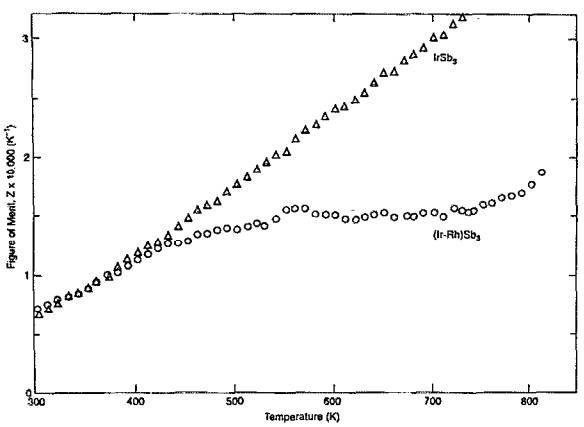

FIG. 8. The figure-of-merit Z as a function of temperature for $IrSb_3$ and $(Ir_{0.5}\,Rh_{0.5})\,Sb_3$.

TABLE II. Infrared active lattice vibrational modes in $CoSb_3$, $RhSb_3$, and $IrSb_3$.

Compound	Vibrational mode energy (cm^{-1})							Reference
$CoSb_3$	275	257	247	174	144	120	78	12
$RhSb_3$	243	225	215			115		13
$IrSb_3$	213	197	187	144	132	112		Present work

from Fig. 4. The ratio $K(\theta)/K'(\theta)=1.7$, which is considered[24] reasonable agreement between theory and experiment for crystals with such a large number of atoms per unit cell.

The minimum thermal conductivity at high temperatures, K_{MIN^∞}, can also be estimated from a Debye approximation[24] as

$$K_{MIN}(\text{acoustic})=\frac{3}{2}\left(\frac{4\pi}{3}\right)^{1/3}\left(\frac{vk}{\delta^2 n_c^{2/3}}\right), \tag{7}$$

$$K_{MIN}(\text{optic})=\frac{k^2\theta}{2h\delta}\left(1+\frac{1}{n_c^{1/3}}\right), \tag{8}$$

where n_c is the number of atoms in a primitive unit cell. The optic contribution is calculated from a sum of $3(n_c-1)$ equally spaced optic modes. The sum of these is

$$K_{MIN^\infty}=(1.87+2.12)\ \text{mW/cm K},$$
$$K_{MIN^\infty}=3.99\ \text{mW/cm K}. \tag{9}$$

The high-temperature region for this calculation is $T\geqslant\theta$. Thus the measured thermal conductivity of $IrSb_3$ at $T=\theta$ is 40 times larger than the minimum.

The lattice thermal conductivity of the mixed crystal $Ir_{0.5}Rh_{0.5}Sb_3$ is also given in Fig. 4. Although the Rh addition decreases the lattice thermal conductivity to 58% of its original value (at room temperature), it comes nowhere close to producing a minimum thermal conductivity sample. Since 1977 there have been a number of studies[26,27] of so-called "filled skutterudites" where various metal atoms have been introduced into the 12-coordinated (with Sb) sites. These sites are very large, and such filling atoms often appear[28–30] to have large thermal vibration parameters. The introduction of such filling atoms may turn out to be an effective method of reducing the lattice thermal conductivity of $IrSb_3$ to values close to K_{MIN} because the "rattling" atoms will strongly scatter the propagating lattice phonons that are responsible for most of the heat transport.

E. Optical reflectivity

The normal incidence optical reflectivity in the far infrared of $IrSb_3$ is shown in Fig. 3. The minima in the curve correspond to transverse optic lattice vibrations.[13] In Table II we have collected the present data for $IrSb_3$ together with literature data[12,13] for $RhSb_3$ and $CoSb_3$. A mode analysis[12] shows that there should be a total of seven infrared-active modes, as were found for $CoSb_3$. Some of these have not been seen in $RhSb_3$ and $IrSb_3$.

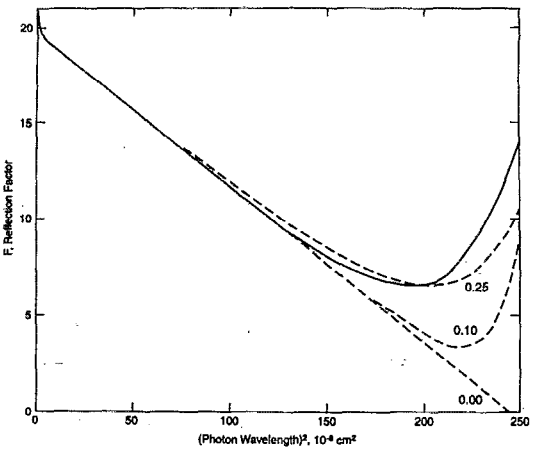

FIG. 9. The experimental reflectivity factor F as a function of the square of the photon wavelength for $IrSb_3$ shown as a solid line. The dashed lines are computed values of F for various ratios of the damping coefficient g to the plasma resonance frequency ω_p. The solid line was determined experimentally.

As pointed out by Kliche and Bauhofer[13] the energies of the higher-energy modes in Table II change noticeably with the mass of the metal atom, indicating that these are metal-antimony vibrations. The lower-energy modes are almost independent of the mass of the metal atom, and are essentially antimony-antimony vibrations.

The reflectivity of $IrSb_3$ for the range $220\ \text{cm}^{-1}\leqslant\bar{\nu}\leqslant 12\,000\ \text{cm}^{-1}$ as shown in Fig. 2 is determined by the free carriers in the sample. Let us define a reflectivity factor[31] F, which is

$$F=\frac{1+\sqrt{R}}{1-\sqrt{R}}. \tag{10}$$

Using the R values from Fig. 2 we have computed F and plotted it as a function of the square of the photon wavelength, λ, in Fig. 9. The linearly extrapolated value of F at zero wavelength is

$$\epsilon_\infty=19.8. \tag{11}$$

The linear extrapolation of F vs λ^2 at $F=0$ is the plasma resonance wavelength:

$$\lambda_p^2=2.42\times10^{-6}\ \text{cm}^2,$$
$$\bar{\nu}_p=(1/\lambda_p)=643\ \text{cm}^{-1}. \tag{12}$$

For comparison of ϵ_∞ values we note that Kliche and Lutz[31] found $\epsilon_\infty=25$ for $CoSb_3$ at room temperature, while Kliche and Bauhofer[13] found $\epsilon_\infty=27$ for $RhSb_3$.

The complex refraction index[32] of $IrSb_3$ is given by

$$n+ik,$$

where n is the real part of the refractive index and k is the imaginary part. In the present case, where there is one plasma resonance frequency ω_p which is considerably higher than any of the phonon frequencies, the theoretical expressions for n and k are[33]

$$n^2-k^2=\epsilon_\infty\left(1-\frac{\omega_p^2}{\omega_p^2+g^2}\right),$$
$$2nk=\epsilon_\infty\left[\frac{\omega_p^2\gamma}{\omega(\omega^2+g^2)}\right]. \quad (13)$$

The plasma damping coefficient is g. The plasma resonance frequency is given in MKSA units by[34]

$$\omega_p=\sqrt{Nq^2/m^*\epsilon_\infty\epsilon_0}, \quad (14)$$

where N=free-carrier concentration, m^*=effective mass of the carriers, q=charge on the electron, and ϵ_0=permittivity of free space. Since the $IrSb_3$ sample is p type with $1.1\times10^{19}/cm^3$ carriers, the effective mass calculated from Eq. (14) is

$$m^*/m_0=0.12, \quad (15)$$

where m_0=the free-electron mass.

We can derive an effective mass value from the Seebeck coefficient at room temperature ($S=72$ μV/K) if we assume[35] that there is a single valence band and that the carriers are scattered by lattice vibrations:[34]

$$S=+\frac{k}{q}\left[\frac{2F_1(\delta^*)}{F_0(\delta^*)}-\delta^*\right],$$
$$\left(\frac{m^*}{m_0}\right)^{3/2}F_{1/2}(\delta^*)=p/N_0(T), \quad (16)$$
$$N_0(T)=\frac{4\pi(2m_0k_BT)^{3/2}}{h^3}.$$

Here δ^*=the reduced Fermi level$=\eta/k_BT$, $F(\delta^*)$ are Fermi functions, k_B=Boltzmann's constant h=Planck's constant, and T=absolute temperature. The result is

$$m^*/m_0=0.17. \quad (17)$$

We believe that the optical reflectivity value for m^* is the better of the two because it does not depend on assumptions about the carrier scattering mechanisms.

F. Optical damping and mobility

The plasma damping coefficient g in Eq. (13) determines the long-wavelength shape of the curve in Fig. 9. The three dashed lines were computed for the ratios:

$$(g/\omega_p)=0.00,\ 0.10,\ \text{or}\ 0.25.$$

The best fit is for

$$(g/\omega_p)=0.25. \quad (18)$$

For $g=0$ we obtain the extrapolated value of λ_p given in Eq. (12).

The optical mobility is given by

$$\mu(\text{opt})=q\tau/m^* \quad (19)$$

and the scattering time τ is

$$\tau=2\pi/g.$$

From Eq. (18) we obtain $\tau=2.08\times10^{-13}$ s, which yields

$$\mu(\text{opt})=3050\ \text{cm}^2/\text{V s}. \quad (20)$$

This value is for a mechanically polished surface, not an electropolished surface. We expect that an undamaged electropolished surface would yield somewhat larger values of μ(opt). The Hall data on this polycrystalline $IrSb_3$ give a measured mobility of

$$\mu(\text{Hall})=1320\ \text{cm}^2/\text{V s}.$$

This lower value for the macroscopic mobility is probably caused by carrier scattering at the grain boundaries.

The present optical data yield a value of

$$U(\text{opt})=\mu(m^*/m_0)^{3/2}=127\ \text{cm}^2/\text{V s}. \quad (21)$$

for the weighted mobility.

V. CONCLUSIONS

The properties of polycrystalline $IrSb_3$ given in Table I suggest that it is an interesting thermoelectric material. The highest value of Z found in unoptimized material was $Z=3\times10^{-4}$ K at 700 K. The p-type samples have rather high carrier mobilities. The undoped samples have a lattice thermal conductivity at room temperature 40 times larger than the minimum value. If the minimum value can be approached by inserting impurities into the lattice voids, better thermoelectric properties may be possible. Further work aimed at making n-type polycrystalline samples, and n-type and p-type single-crystal samples seems desirable in order to further evaluate its potential.

ACKNOWLEDGMENTS

The authors wish to thank Hugh Woodbury and Robert Lewandowski for making the measurements shown in Figs. 5, 6, and 7, Peter Codella for the measurements in Figs. 2 and 3, Cindy Haydn for the measurements in Fig. 1, and Robert Gilmore for the sound velocity data.

[1] I. Oftedal, Norsk Geol. Tidsskr **8**, 250 (1925); Z. Krist. **66**, 517 (1928).
[2] N. N. Zhuravlev and G. S. Zhdanov, Kristallogr. **1**, 509 (1956) [Sov. Phys. Cryst. **1**, 404 (1956)].
[3] A. Kjekshus and G. Pedersen, Acta Crystallogr. **14**, 1065 (1961).
[4] F. Hulliger, Helv. Phys. Acta **34**, 782 (1961).
[5] D. Jung, M. H. Whangbo, and S. Alvarez, Inorg. Chem. **29**, 2252 (1990).
[6] L. Pauling and M. L. Huggins, Z. Krist. **87**, 205 (1934).
[7] T. Caillat, A. Borshchevsky, and J. P. Fleurial, *Proceedings of the Eleventh International Conference on Thermoelectrics, Arlington, Texas, 1993*, edited by K. R. Rao (University of Texas Press, Arlington, 1993).
[8] R. N. Kuzmin, G. S. Zhdanov, and N. N. Zhuravlev, Kristallogr. **2**, 48 (1957) [Sov. Phys. Cryst. **2**, 42 (1957)].
[9] A. Kjekshus, Acta Chem. Scand. **15**, 678 (1961).
[10] A. Kjekshus and T. Rakke, Acta Chem. Scand. A **28**, 99 (1974).
[11] O. L. Anderson, J. Phys. Chem. Solids **24**, 909 (1963).
[12] H. D. Lutz and G. Kliche, Phys. Status Solidi B **112**, 549 (1982).
[13] G. Kliche and W. Bauhofer, Mater. Res. Bull. **22**, 551 (1987).
[14] L. D. Dudkin and N. Kh. Abrikosov, Zhurn. Neorg. Khim. **1**, 2096 (1956) [Russ. J. Inorg. Chem. **1**(9), 169 (1956)].
[15] D. Greig, Phys. Rev. **120**, 358 (1960).
[16] A. D. Stukes, Br. J. Appl. Phys. **12**, 675 (1961).
[17] E. D. Devyatkova, A. V. Petrov, and I. A. Smirnov, Fiz. Tverd. Tela **3**, 1338 (1961) [Sov. Phys. Solid State **3**, 970 (1961)].
[18] S. S. Shalyt, V. M. Mozhdaba, and A. D. Galetskaya, Fiz. Tverd. Tela **10**, 1277 (1968) [Sov. Phys. Solid State **10**, 1018 (1968)].
[19] E. F. Steigmeier, in *Thermal Conductivity*, edited by R. P. Tye (Academic, New York, 1969), Vol. 2, Chap. 4.
[20] E. Grüneisen, in *Handbuch der Physik*, edited by H. Geiger and K. Scheel (Springer, Berlin, 1926), Vol. 10, pp. 1–59.

[21] J. A. Beattie, J. Math. Phys. **6**, 1 (1926-27).
[22] A. Okazaki and M. Kawaminami, Mater. Res. Bull. **8**, 545 (1973).
[23] T. Soma and K. Kudo, J. Phys. Soc. Jpn. **48**, 115 (1980).
[24] G. A. Slack, in *Solid State Physics*, edited by H. Ehrenreich, F. Seitz, and D. Turnbull (Academic, New York, 1979), Vol. 34, p. 1.
[25] H. D. Lutz and G. Kliche, Z Anorg. Allg. Chem. **480**, 105 (1981).
[26] W. Jeitschko and D. Braun, Acta Crystallogr. B **33**, 3401 (1977).
[27] N. D. Stetson, S. M. Kauzlarich, and H. Hope, J. Solid State Chem. **91**, 140 (1991).
[28] D. J. Braun and W. Jeitschko, J. Less-Common Met. **72**, 147 (1980).
[29] L. E. DeLong and G. P. Meisner, Solid State Commun. **53**, 119 (1985).
[30] L. Boonk, W. Jeitschko, U. D. Scholz, and D. J. Braun, Z. Kristallogr. **178**, 30 (1987).
[31] G. Kliche and H. D. Lutz, Infrared Phys. **24**, 171 (1984).
[32] D. T. F. Marple, J. Appl. Phys. **35**, 1879 (1964).
[33] F. Stern, Solid State Phys. **15**, 299 (1963).
[34] E. D. Palik, *Handbook of Optical Constants of Solids* (Academic, New York, 1985), p. 552.
[35] G. A. Slack and M. A. Hussain, J. Appl. Phys. **70**, 2694 (1991).